EPJ B
Condensed Matter and Complex Systems
EPJ.org
your physics journal

Eur. Phys. J. B (2018) 91: 89 DOI: 10.1140/epjb/e2018-90030-0

Stability of two-mode internal resonance in a nonlinear oscillator

Damián H. Zanette

edp sciences
Società Italiana di Fisica
Springer

Eur. Phys. J. B (2018) 91: 89
https://doi.org/10.1140/epjb/e2018-90030-0

THE EUROPEAN PHYSICAL JOURNAL B

Regular Article

Stability of two-mode internal resonance in a nonlinear oscillator

Damián H. Zanette[a]

Centro Atómico Bariloche (Comisión Nacional de Energía Atómica) and Instituto Balseiro (Universidad Nacional de Cuyo), Consejo Nacional de Investigaciones Científicas y Técnicas, 8400 San Carlos de Bariloche, Río Negro, Argentina

Received 18 January 2018 / Received in final form 26 March 2018
Published online 23 May 2018 – © EDP Sciences, Società Italiana di Fisica, Springer-Verlag 2018

Abstract. We analyze the stability of synchronized periodic motion for two coupled oscillators, representing two interacting oscillation modes in a nonlinear vibrating beam. The main oscillation mode is governed by the forced Duffing equation, while the other mode is linear. By means of the multiple-scale approach, the system is studied in two situations: an open-loop configuration, where the excitation is an external force, and a closed-loop configuration, where the system is fed back with an excitation obtained from the oscillation itself. The latter is relevant to the functioning of time-keeping micromechanical devices. While the accessible amplitudes and frequencies of stationary oscillations are identical in the two situations, their stability properties are substantially different. Emphasis is put on resonant oscillations, where energy transfer between the two coupled modes is maximized and, consequently, the strong interdependence between frequency and amplitude caused by nonlinearity is largely suppressed.

1 Introduction

The joint dynamics of mutually interacting oscillators is a problem of high relevance to broad areas within physics, chemistry, and biology, as well as to technological applications [1,2]. In the field of Continuum Mechanics, coupled oscillator systems are at the basis of the modeling of vibrations in structures of all kinds. The oscillatory dynamics of solid beams, which was one of the foundational problems of continuum mechanics [3], has recently regained much interest in view of its applications to microtechnologies [4–6]. In fact, micromechanical oscillators in the form of tiny silica bars – which are readily built during circuit printing, and are actuated by very small electric fields – can be incorporated to miniaturized equipment, as components of sensors and time-keeping devices [7].

To overcome the effects of thermal and electronic noise, micromechanical oscillators must work within a regime of large oscillation amplitude, where nonlinear effects are unavoidable [8]. This brings about an undesirable interdependence between the oscillation frequency and the amplitude, which is obviously noxious for time keeping-devices: any amplitude fluctuation – caused, for instance, by noise, or by uncontrolled changes of a parameter – will bring about a variation in the frequency, with the consequent loss of precision in the clock. However, for micromechanical oscillators consisting of a beam clamped at its two ends, it has been recently discovered that the frequency-amplitude interdependence can be drastically reduced if the main oscillation mode resonates with a higher-harmonic mode – a phenomenon called internal resonance. Under such conditions, the main oscillation mode is able to efficiently transfer any energy surplus to the other mode, thus damping the effect of amplitude fluctuations and stabilizing the frequency [5].

Internal resonance is a well-known phenomenon in the vibration of solid bodies, where two (or more) oscillation modes synchronize with each other thanks to the coupling which derives from nonlinearity [9]. Its application to frequency stabilization, as described in the preceding paragraph, naturally requires that these synchronized resonant oscillations are stable forms of periodic motion. In this paper, we analyze the stability of synchronized motion of two oscillation modes in the non-standard situation where the main mode is excited by a force generated by the oscillator itself. In fact, for the system to generate an autonomous frequency – as required in any time-keeping device [10] – a conditioned version of a signal read from the same oscillator is reinjected as excitation. This self-sustained (closed-loop) configuration contrasts with the standard situation of an externally forced oscillator (open-loop configuration), where the frequency is fixed from outside the system.

In Section 2, we introduce the two-oscillator model used to describe the resonant interaction between the two modes. Focusing on a solid beam clamped at its two ends [5], the main mode is represented by a nonlinear Duffing oscillator – much as for a clamped-clamped vibrating string [11,12]. The higher-harmonic mode, on the other hand, is linear. Equations of motion for the (slow) dynamics of oscillation amplitudes and phases are formulated within the multiple-scale approximation [9].

[a] e-mail: zanette@cab.cnea.gov.ar

Section 3 begins with the analysis of stationary oscillations, which are identical for both closed- and open-loop configurations. Then, the stability in the standard open-loop configuration is studied as a reference case and, finally, stability in the closed-loop configuration is analyzed. In view of the application to frequency stabilization in nonlinear micromechanical oscillators, the study is focused in the parameter ranges where internal resonance is realized. Section 4 is devoted to a summary of our results and to some final remarks.

2 Two-oscillator model

As advanced in the Introduction, a traditional model for the interaction between two oscillation modes in a vibrating beam consists of two coupled one-dimensional mechanical oscillators, described by coordinates $x_1(t)$ and $x_2(t)$. In our case, the main oscillation mode is represented by an oscillator of natural frequency ω_1 with a cubic (Duffing) nonlinearity in its restoring force. By a suitable choice of time units, we fix $\omega_1 = 1$. Moreover, the main oscillation mode is excited by a harmonic force $F_\Omega(t)$ with frequency Ω. The secondary, higher-harmonic mode, in turn, is represented by a linear oscillator with natural frequency ω_2. The interaction between the two oscillators is assumed to be linear, as derived, for instance, from a bilinear potential $V_{\rm int}(x_1, x_2) = J_{\rm int} x_1 x_2$. The equations of motion, normalized by the respective masses $m_{1,2}$, are

$$\ddot{x}_1 + \gamma_1 \dot{x}_1 + \left(1 + \frac{4}{3}\beta x_1^2\right) x_1 = J x_2 + f_\Omega(t), \qquad (1)$$

and

$$\ddot{x}_2 + \gamma_2 \dot{x}_2 + \omega_2^2 x_2 = J x_1, \qquad (2)$$

where $\gamma_{1,2}$ are the damping coefficients per unit mass, β is the Duffing coefficient, $f_\Omega(t) = m_1^{-1} F_\Omega(t)$, and $x_2(t)$ has been rescaled in such a way that the coupling coefficient J is the same in both equations.

Naturally, due to nonlinearity, equations (1) and (2) cannot be exactly solved. An approximate solution, however, can be systematically constructed by assuming that the time scales associated with oscillations, of order $\omega_{1,2}^{-1}$, Ω^{-1}, are much shorter than the time scales associated with the relaxation of oscillation amplitudes and phases toward their stationary values, of order $\gamma_{1,2}^{-1}$. This assumption is indeed satisfied in a broad class of important applications, including the dynamics of micromechanical oscillators, for which the quality factor $Q = \omega/\gamma$ can be of order 10^4 or larger [5]. Under these conditions, it is possible to propose solutions of the form $x_{1,2}(t) = A_{1,2}(t)\cos[\Omega t + \phi_{1,2}(t)]$, where $A_{1,2}(t)$ and $\phi_{1,2}(t)$ evolve over scales much longer than the oscillation periods. The first-order approximation, which is obtained keeping harmonic contributions of frequency Ω, yields the following equations for amplitudes and phases:

$$\begin{aligned}
2\Omega \dot{A}_1 &= -\gamma_1 \Omega A_1 + J A_2 \sin(\phi_2 - \phi_1) - f_s, \\
2\Omega A_1 \dot{\phi}_1 &= (1 - \Omega^2 + \beta A_1^2) A_1 - J A_2 \cos(\phi_2 - \phi_1) - f_c, \\
2\Omega \dot{A}_2 &= -\gamma_2 \Omega A_2 - J A_1 \sin(\phi_2 - \phi_1), \\
2\Omega A_2 \dot{\phi}_2 &= (\omega_2^2 - \Omega^2) A_2 - J A_1 \cos(\phi_2 - \phi_1), \qquad (3)
\end{aligned}$$

where $f_{c,s}$ are defined by introducing the decomposition $f_\Omega(t) = f_c \cos(\Omega t + \phi_1) + f_s \sin(\Omega t + \phi_1)$. Their explicit form will be obtained later for each case of interest. The multiple-scale approximation used to obtain equations (3) formally requires that all the forces acting on the oscillators are small as compared to the linear restoring force, and that all the frequencies involved in the problem are similar to each other, $\omega_1 \approx \omega_2 \approx \Omega$ [9]. Comparison with numerical solutions to the equations of motion shows however that, in practice, the method yields excellent approximations over much less stringent conditions [13].

3 Stationary oscillations and their stability

Fixed points of equations (3) correspond to stationary oscillatory motion where $x_1(t)$, $x_2(t)$ and the excitation $f_\Omega(t)$ are synchronized at frequency Ω. Irrespectively of the form of $f_\Omega(t)$, the last two of equations (3) make it possible to solve the stationary problem for the amplitude A_2 and the phase difference $\psi = \phi_2 - \phi_1$ in terms of the other variables, as

$$\begin{aligned}
A_2 \cos\psi &= (\omega_2^2 - \Omega^2) J A_1 / [(\omega_2^2 - \Omega^2)^2 + \gamma_2^2 \Omega^2], \\
A_2 \sin\psi &= -\gamma_2 \Omega J A_1 / [(\omega_2^2 - \Omega^2)^2 + \gamma_2^2 \Omega^2], \qquad (4)
\end{aligned}$$

which, in turn, implies

$$A_2 = \frac{|J| A_1}{\sqrt{(\omega_2^2 - \Omega^2)^2 + \gamma_2^2 \Omega^2}}. \qquad (5)$$

It is clear from this result that x_2 responds resonantly to its coupling to x_1, with maximal response when $\Omega \approx \omega_2$. The ratio A_2/A_1 is proportional to the coupling strength J and, as a function of Ω, follows the typical linear resonance peak profile of width γ_2 around ω_2.

Replacing equations (4) into the stationary version of the first two of equations (3), the remaining unknowns can be found. This, however, requires to specify the form of the excitation $f_\Omega(t)$. As advanced, we here consider two cases, corresponding to different setups in which internal resonance can be realized: (I) an open-loop configuration, where the oscillator is excited by an external force, and (II) a closed-loop configuration, where the excitation is a self-sustaining force generated from a signal read from the same oscillator, with fixed amplitude and phase shift.

3.1 Case I: Open-loop configuration

Case I corresponds to the standard situation where the system is excited by a harmonic force with externally controlled amplitude and frequency. Taking $f_\Omega(t) =$

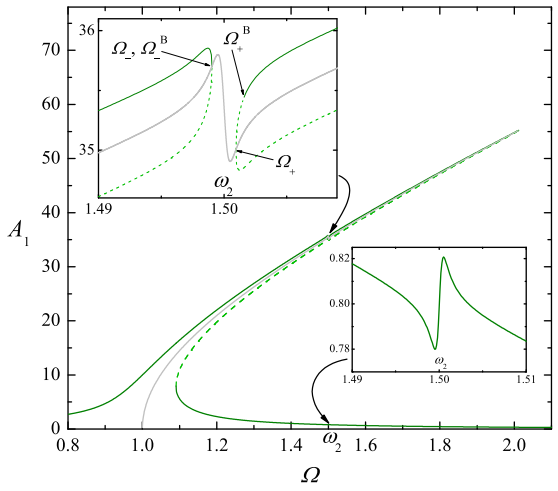

Fig. 1. Stationary solution of equations (3) for the oscillation amplitude A_1 as a function of the excitation frequency Ω (case I). Parameter values are $\gamma_1 = 0.009$, $\beta = 0.001$, $f_0 = 1$, $J = 0.01$, $\omega_2 = 1.5$, and $\gamma_2 = 0.001$. Full and dashed lines correspond to stable and unstable solutions, respectively. Thin light lines stand for the backbone curve. The insets are close-ups of the zones indicated by the arrows. In the upper-left inset, which shows the resonance gap at $\Omega \approx \omega_2$, $\Omega_\pm$ are the frequencies at the intersections between $A_1(\Omega)$ and the backbone curve, while $\Omega_\pm^{\rm B}$ are the frequencies at the boundaries between stable and unstable solutions. Note that, to the plot resolution, Ω_- and $\Omega_-^{\rm B}$ coincide.

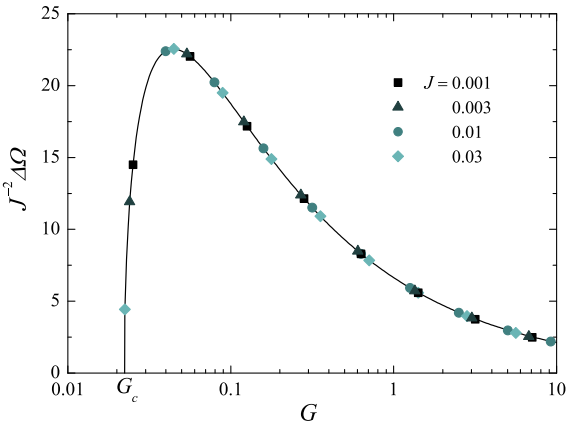

Fig. 2. Scaled gap width, $J^{-2}\Delta\Omega = J^{-2}(\Omega_+ - \Omega_-)$, as a function of the parameter combination $G = J^2/\gamma_2$. The curve corresponds to the approximation given by equation (8), and symbols stand for the evaluation of $\Omega_\pm$ from the exact stationary solution to equations (3), as the intersection between the solution and the backbone curve (see Fig. 1), for several values of J. Other parameters are as in Figure 1. Increasing G, the gap opens at the critical value G_c.

$f_0 \cos \Omega t$, in equations (3) we have $f_s = f_0 \sin\phi_1$ and $f_c = f_0 \cos\phi_1$. Once solutions (4) have been obtained, the first two of equations (3) can be used to find A_1 and ϕ_1 in the stationary states. The stationary solution for the amplitude A_1 as a function of the excitation frequency Ω has the overall form of the well-known Duffing resonance curve [12], as shown in the main panel of Figure 1. However, due to the resonant transfer of energy between the oscillators when $\Omega \approx \omega_2$, a gap opens in the curve (upper-left inset) [5,13]. For values of Ω inside this resonance gap, the only accessible value of A_1 lies on the low-amplitude branch, which locally develops a double peak (lower-right inset).

As a function of Ω, A_1^2 is the root of a third-order polynomial equation, with one or three real positive solutions. Working out their analytical expressions is impractical, but accurate approximations can be obtained for the solutions along the upper branches of the Duffing peak when the peak is narrow enough. These approximate solutions read

$$A_1^2(\Omega) = \frac{\Omega^2 - 1 + u_c}{\beta} \pm \frac{1}{\beta}\sqrt{\frac{\beta f_0^2}{\Omega^2 - 1} - (\gamma_1\Omega + u_s)^2}, \quad (6)$$

with

$$u_c(\Omega) = (\omega_2^2 - \Omega^2)J^2/[(\omega_2^2 - \Omega^2)^2 + \gamma_2^2\Omega^2],$$
$$u_s(\Omega) = \gamma_2\Omega J^2/[(\omega_2^2 - \Omega^2)^2 + \gamma_2^2\Omega^2]. \quad (7)$$

The square root of the first term in the right-hand side of equation (6), $\bar{A}_1(\Omega) = \sqrt{[\Omega^2 - 1 + u_c(\Omega)]/\beta}$ gives the so-called backbone curve. It has been plotted as a thin line in Figure 1. The backbone curve is always situated between the two upper branches of the Duffing resonance peak, thus providing a stylized representation of its overall shape.

As shown in the upper-left inset of Figure 1, the frequencies $\Omega_\pm$ at the intersections between the solution $A_1(\Omega)$ and the backbone curve can be used to estimate the position and width of the resonance gap. For $\Omega \in (\Omega_-, \Omega_+)$, the argument of the square root in equation (6) is negative. When the quality factor $Q_2 = \omega_2/\gamma_2$ is sufficiently large, the function $u_s(\Omega)$ attains significant values only in the close vicinity of ω_2. This makes it possible to give an explicit approximate expression for $\Omega_\pm$, as

$$\Omega_\pm \approx \omega_2 \pm \frac{\gamma_2}{2}\sqrt{\frac{J^2/\gamma_2\omega_2}{\sqrt{\beta f_0^2/(\omega_2^2 - 1)} - \gamma_1\omega_2} - 1}. \quad (8)$$

Within this approximation, the gap width $\Delta\Omega = \Omega_+ - \Omega_-$ vanishes when

$$\frac{J^2}{\gamma_2} = \omega_2\sqrt{\frac{\beta f_0^2}{\omega_2^2 - 1}} - \gamma_1\omega_2^2 \equiv G_c. \quad (9)$$

Therefore, for given parameters in the equation of motion for x_1 and a fixed value of ω_2, the opening of the gap takes place when the combination $G = J^2/\gamma_2$ becomes larger than the critical value G_c. In other words, the resonance gap occurs when the coupling strength J is large enough or, equivalently, when the damping coefficient γ_2 is sufficiently small.

Figure 2 shows the scaled gap width $J^{-2}\Delta\Omega$ as a function of the combination $G = J^2/\gamma_2$. The curve

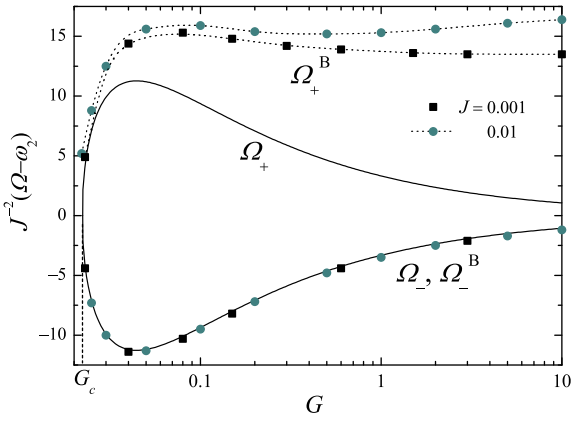

Fig. 3. Symbols: the frequencies $\Omega_\pm^B$ at the boundary between stable and unstable oscillations vs. $G = J^2/\gamma_2$, for two values of J. Other parameters are as in Figure 1. Dashed lines are B-spline interpolations, plotted as a guide to the eye. Full lines: gap boundaries, $\Omega_\pm$, given by equation (8). In the vertical axis, Ω is measured with respect to ω_2 and, as in Figure 2, is rescaled by a factor J^{-2}.

corresponds to the approximation given by equation (8), while symbols stand for the numerical evaluation of the width from the stationary solutions to equations (3) for various values of the coupling strength J, with $\Omega_\pm$ given by the intersection between the solution and the backbone curve, as defined above. The coincidence with the approximation is excellent. As G grows – i.e. as the interaction becomes stronger, and/or the damping coefficient γ_2 decreases – the gap broadens rapidly for $G \gtrsim G_c$, it attains a maximal width, and then becomes progressively narrower, with $J^{-2}\Delta\Omega \propto G^{-1/2}$ for large G.

Regarding the stability of the stationary states, full and dashed lines in Figure 1 represent stable and unstable solutions, respectively. Linear stability of fixed points is assessed in the usual way, by determining the Jacobian eigenvalues for system (3). Being the roots of a fourth-degree polynomial, the eigenvalues could in principle be found analytically. In practice, however, a numerical evaluation for each parameter set must be performed. As is well known to happen with the externally forced Duffing oscillator, for the values of Ω for which three solutions for the amplitude exist, the two outer solutions are stable while the one in the middle is unstable [9,12]. The upper-left inset in Figure 1 shows how the stable and unstable branches extend inside the resonance gap. We see that, to the left of the gap ($\Omega < \omega_2$), the boundary Ω_-^B between stable and unstable solutions practically coincides with the intersection Ω_- between the curve $A_1(\Omega)$ and the backbone curve. Analysis of the eigenvalue dependence on the parameters shows that this boundary is associated to a saddle-node bifurcation. On the other hand, to the right of the gap ($\Omega > \omega_2$), unstable solutions invade the upper branch of the resonance curve, so that the boundary Ω_+^B between stable and unstable solutions lies on the upper branch, clearly to the right of the intersection Ω_+ between $A_1(\Omega)$ and the backbone curve. In this case, the stability transition is a subcritical Hopf bifurcation.

To characterize these properties for other parameter sets, we have detected the boundaries $\Omega_\pm^B$ between stable and unstable solutions for several values of G and two of the values of the coupling strength J considered in Figure 2. Results are shown in Figure 3, where full lines correspond to the gap ends $\Omega_\pm$ calculated from equation (8) and symbols stand for numerical estimation of $\Omega_\pm^B$. In the plot, frequencies are measured with respect to ω_2 and rescaled as in Figure 2. We see that, for $\Omega < \omega_2$, Ω_-^B and Ω_- are virtually coincident. This indicates that, to the left of the gap, stable and unstable solutions are respectively confined to the upper and lower branches of the resonance curve. Moreover, this boundary is always associated to a saddle-node bifurcation.

On the other hand, for $\Omega > \omega_2$, the boundary Ω_+^B is well above Ω_+, indicating that unstable solutions occupy part of the upper branch, as illustrated in the upper-left inset of Figure 1. Note that Ω_+^B does not verify the same scaling with J as all the other data shown in the plot (and in Fig. 2). In fact, results for different J lie on different curves, although their mutual deviation is not very large for these values of the coupling strength. Note also that, for sufficiently large G, the boundary slightly shifts to larger frequencies in spite of the fact that the gap is increasingly narrower. For all the parameter sets studied here, Ω_+^B corresponds to a subcritical Hopf bifurcation.

3.2 Case II: Closed-loop configuration

In time-keeping devices, such as clocks and pacemakers, the emergence of an autonomously generated frequency – not depending on the action of an external periodic force – is achieved by exciting the mechanical oscillator with a force which results from conditioning a signal read from the oscillator itself. In modern clocks, this self-sustaining force is generated and reinjected into the system using an electronic circuit. The circuit reads the phase of the main oscillation mode, ϕ_1, and generates a signal with the same phase shifted by a fixed amount ϕ_0, and a fixed amplitude f_0 [10]. Thus, in equation (1) we have $f_\Omega(t) = f_0\cos(\phi_1+\phi_0)$ while, in equations (3), $f_s = -f_0\sin\phi_0$ and $f_c = f_0\cos\phi_0$.

Once equations (4) have been replaced into the right-hand sides of equations (3), the stationary version of the first two of these equations has the same form as in case I, except that in $f_{c,s}$ the phase ϕ_1 is replaced by $-\phi_0$. In contrast with case I, however, the unknowns in these equations are A_1 and Ω, and ϕ_0 is a control parameter fixed by the conditioning of the oscillator signal. The oscillation frequency Ω emerges now from the interplay between the internal dynamics of the system and the self-sustaining force.

Notwithstanding these differences, it is not difficult to realize that, in the present case, the interdependence between the stationary values of A_1 and Ω is exactly the same as in case I. Indeed, once ϕ_1 (in case I) or ϕ_0 (in case II) are eliminated from the first two of equations (3), the respective functional relations between A_1 and Ω are identical. In particular, this means that – disregarding the information about stability – the curves shown in

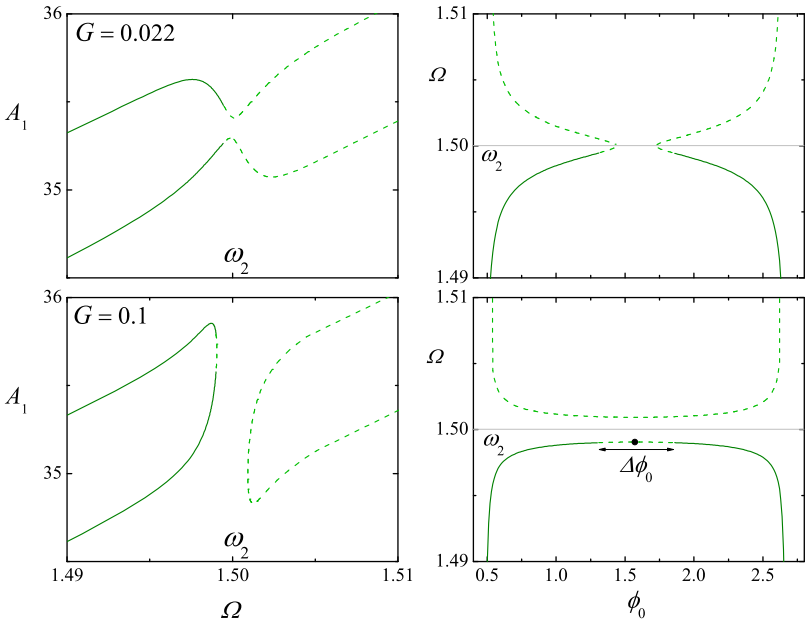

Fig. 4. Upper panels: A_1 vs. Ω (left) and Ω vs. ϕ_0 (right) in the resonance zone, for case II. Full and dashed lines correspond to stable and unstable solutions, respectively. The combination $G = J^2/\gamma_2 = 0.022$ is just below the critical value $G_c \approx 0.0222$ at which the gap opens. Other parameters are as in Figure 1. Lower panels: as in the upper panels, for $G = 0.1$, with the gap already opened. The horizontal lines in the rightmost panels indicate the value of ω_2. In the lower plateau of the lower-right plot, the dot at $\phi_0 = \pi/2$ indicates the state s_0, whose stability is discussed in the text. The unstable segment around s_0 has width $\Delta\phi_0$.

Figures 1 and 2 hold in both cases. Similarly, the approximations given by equations (6) to (9) are also valid for case II.

On the other hand, stability properties are not the same for the two cases. In case I, in fact, the terms $f_{c,s}$ in equations (3) depend on ϕ_1, which is one of the dynamical variables of the system, while in case II they are constants determined by the control parameters f_0 and ϕ_0. This difference has direct impact in the form of the Jacobian and, therefore, of its eigenvalues. For case II, it has been shown that, in the absence of coupling between the oscillators ($J = 0$), stationary oscillations of x_1 are stable for any $\phi_0 \in (0, \pi)$, i.e. along the whole resonance curve, independently of how many solutions for A_1 exist for each value of Ω [10,13]. When coupling is present, as shown below, the opening of the resonance gap is preceded by the appearance of a zone of instability around $\Omega = \omega_2$, which persists when the gap has opened. In contrast with case I, all the transitions between stable and unstable solutions are now subcritical Hopf bifurcations.

The two upper panels in Figure 4 show A_1 vs. Ω (left) and Ω vs. ϕ_0 (right) in the resonance region, for a value of the combination $G = J^2/\gamma_2$ just below $G_c \approx 0.0222$, namely, $G = 0.022$. The gap has not opened yet, but an instability zone (dashed curves) has developed around $\Omega = \omega_2$. For $G = 0.1$, as shown by the lower panels, the gap has now opened, and unstable solutions persist at both sides of the gap.

It is clear from the lower-right panel that, for $G > G_c$, the frequency Ω inside the gap exhibits two plateaus at each side of ω_2 where, over a wide interval of ϕ_0, its dependence with the phase shift is much smoother than anywhere outside the gap. This is the zone of frequency stabilization referred to in the Introduction, that has been proposed as an operational regime where the variation of Ω on the control parameters, caused by nonlinearity, can be minimized. The frequency of nonlinear oscillators working in this zone exhibits robust behavior against deterministic and random fluctuations of those parameters, which is essential to the functioning of time-keeping devices [5].

For the parameters of Figure 4, the upper plateau inside the gap ($\Omega > \omega_2$) corresponds to unstable solutions. Although we are not able to give a general proof, it turns out that solutions on the upper plateau remain unstable over broad parameter ranges. Meanwhile, most of the lower plateau ($\Omega < \omega_2$) corresponds to stable solutions, except for a segment around $\phi_0 = \pi/2$, where they are unstable. Stability analysis shows however that this unstable segment may disappear for different parameter sets. In particular, it is not present for sufficiently large values of the damping coefficient γ_1 of the main oscillation mode, and appears as γ_1 decreases.

To analyze this behavior, we have determined the stability on the lower plateau at $\phi_0 = \pi/2$, using the criterion that if this particular state is stable, then the unstable segment is absent, and vice versa. For brevity, we denote this state as s_0 (see the dot in the lower-right panel of Fig. 4). Note that s_0 coincides with the intersection between the low-frequency part of the resonance curve and the backbone curve introduced for case I (cf. the upper-left inset of Fig. 1). In particular, we have analyzed the stability

of s_0 as a function of G and J, for several values of γ_1, fixing the other parameters to the values indicated for Figures 1–4. For $\gamma_1 \gtrsim 0.01$, whenever the gap is open, s_0 is stable for any G and J, indicating that the unstable segment is always absent. As the damping coefficient of the main oscillation mode decreases to $\gamma_1 \lesssim 0.0095$, however, a "tongue" appears in the G-J plane, inside which s_0 is unstable. The darkest curve in the upper panel of Figure 5 shows the tongue boundary for $\gamma_1 = 0.0094$. As γ_1 decreases further, the instability zone grows in size, towards large values of G and J. For low G, it is always limited by the value G_c at which the resonance gap opens. The limit for $\gamma_1 = 0$ is well defined, and is shown by the lightest curve. Dark and light hatched regions show the instability zone for $\gamma_1 = 0.0093$ and the stability zone for $\gamma_1 = 0$, respectively.

Within the instability zone corresponding to a given value of γ_1, the width $\Delta\phi_0$ of the unstable segment depends on G and J. To illustrate this dependence, in the lower panel of Figure 5 we plot $\Delta\phi_0$ as a function of G for various values of J and $\gamma_1 = 0.009$. We see that $\Delta\phi_0$ reaches a maximum inside the instability tongue, whose value decreases as J grows. For large J, $\Delta\phi_0$ vanishes at the boundaries of the tongue, while for small J it reaches a finite value at the lower-G end, where $G \approx G_c$.

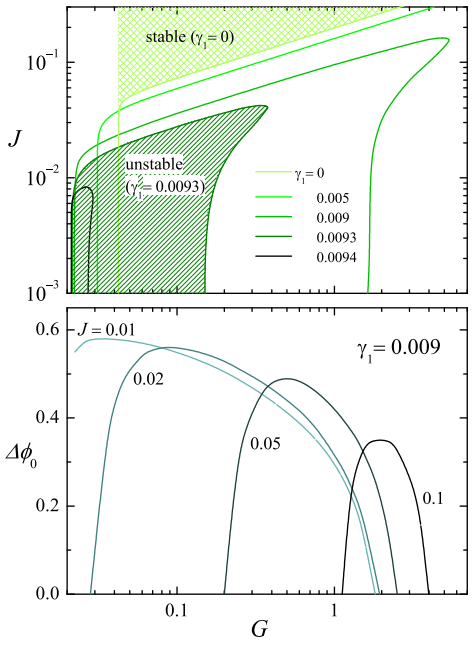

Fig. 5. Upper panel: instability zones for s_0, the state at $\phi_0 = \pi/2$ on the lower plateau inside the resonance gap (see Fig. 4), on the G-J plane, for various values of the damping coefficient γ_1. Hatched regions correspond to the instability zone for $\gamma_1 = 0.0093$ and the stability zone for $\gamma_1 = 0$. Other parameters are as in Figure 1. Lower panel: the width of the unstable segment on the lower plateau, $\Delta\phi_0$, as a function of G, for several values of J and $\gamma_1 = 0.009$.

4 Conclusion

We have analyzed the stability of synchronized periodic motion in a system formed by two coupled mechanical oscillators. One of them is governed by the Duffing equation and is excited by a harmonic force, while the other is linear. They respectively model the main oscillation mode and a higher-harmonic mode of a vibrating solid beam clamped at its two ends. Regarding the harmonic excitation, two cases were studied. On the one hand, we have considered the standard situation where the excitation is an external force with prescribed amplitude and frequency (open-loop configuration) [9,12]. On the other, we have studied the case in which the excitation is a conditioned version of a signal read from the oscillator itself, with prescribed phase shift with respect to the oscillation, and fixed amplitude (closed-loop configuration). This feedback self-sustaining force insures that the oscillation frequency is an emergent property of the system, which thus results to behave as an autonomous pacemaker suitable for time-keeping applications [10].

In the closed-loop configuration and under conditions of internal resonance, where synchronization occurs near the frequency of the higher-harmonic mode, a regime develops where the dependence of the frequency on the control parameters is largely suppressed – much in contrast with the situation outside internal resonance, where nonlinearity determines that the frequency is very sensible to changes in the parameters. Physically, this effect is related to the efficient power transfer that resonance establishes between the oscillation modes, with the higher-harmonic mode acting as a kind of "buffer" for energy variations in the main mode. Functioning within this regime has been proposed as a mechanism of frequency stabilization in micromechanical oscillators [5]. This application motivated our focusing on internal resonance and, in particular, on the parameters that control energy transfer and dissipation – namely, coupling and damping coefficients. Other parameters, such as the higher-harmonic frequency, the cubic restoring force coefficient, and the forcing amplitude, determine the position of internal resonance and how long and leaned the Duffing resonance peak is, but are not expected to play an important role in determining the stability of stationary synchronized oscillations.

We also mention here that all our results have been obtained within the multiple-scale approximation of the equations of motion, which allows for a systematic treatment of nonlinearity. We have verified that these results are in good agreement with direct numerical solutions of equations (1) and (2) – not presented in this paper – for several relevant parameter sets (see also [13]). This agreement is not unexpected, in view that the multiple-scale approximation improves as the time scales of oscillations and of energy dissipation become more separated from each other. As explained in Section 2, this separation is measured by the quality factor which, in the cases presented here, is in the range $Q \sim 10^2$–10^3. In real micro- and nanomechanical oscillators, the quality factor reaches values from 10^4 to 10^8 [5,14], which makes the approximation even more accurate.

A variation of the closed-loop configuration has recently been proposed and tested experimentally, for which the self-sustaining force depends linearly on either the

coordinate or the velocity of the main oscillation mode [15]. Designs based on a linear self-sustaining force may improve control and tunability and, at the same time, decrease power consumption. On the other hand, to give rise to oscillations of finite amplitude, they generally need a certain degree of nonlinearity in the intrinsic mechanisms of energy dissipation [15,16]. As in the case of the self-sustaining force considered here, however, the exploitation of internal resonance to achieve frequency stabilization relies on the stability of the resulting resonant oscillations. Consequently, a natural extension of the present analysis should encompass the study of these forms of linear feedback.

Financial support from ANPCyT, Argentina (Grant PICT 2014-1611), is acknowledged. The author is grateful to S.I. Arroyo, C. Chen, D.A. Czaplewski, J.R. Guest, D. López, F. Mangussi, and S. Shaw for recent collaboration on the present subject.

References

1. A. Pikovsky, M. Rosenblum, J. Kurths, *Synchronization. A universal concept in nonlinear sciences* (Cambridge University Press, Cambridge, 2003)
2. S.C. Manrubia, A.S. Mikhailov, D.H. Zanette, *Emergence of dynamical order. Synchronization phenomena in complex systems* (World Scientific, Singapore, 2004)
3. O.A. Bauchau, J.I. Craig, *Structural analysis* (Springer, Amsterdam, 2009)
4. K.L. Ekinci, M.L. Roukes, Rev. Sci. Instrum. **76**, 061101 (2005)
5. D. Antonio, D.H. Zanette, D. López, Nat. Commun. **3**, 806 (2012)
6. D.K. Agrawal, J. Woodhouse, A.A. Seshia, IEEE Trans. Ultrason. Ferroelectr. Freq. Control **60**, 1646 (2013)
7. J.T.M. van Beek, R. Puers, J. Micromech. Microeng. **22**, 013001 (2012)
8. M. Agarwal, H. Mehta, R.N. Candler, S.A. Chandorkar, B. Kim, M.A. Hopcroft, R. Melamud, G. Bahl, G. Yama, T.W. Kenny, B. Murmann, J. Appl. Phys. **102**, 074903 (2007)
9. A.H. Nayfeh, D.T. Mook, *Nonlinear oscillations* (Wiley, New York, 1995)
10. B. Yurke, D.S. Greywall, A.N. Pargellis, P.A. Busch, Phys. Rev. A **51**, 4211 (1995)
11. T.C. Molteno, N.B. Tufillaro, Am. J. Phys. **72**, 1157 (2004)
12. I. Kovacic, M.J. Brennan, *The Duffing equation: nonlinear oscillators and their behaviour* (Wiley, New York, 2011)
13. S.I. Arroyo, D.H. Zanette, Eur. Phys. J. B **89**, 12 (2016)
14. H.B. Peng, C.W. Chang, S. Aloni, T.D. Yuzvinsky, A. Zettl, Phys. Rev. Lett. **97**, 087203 (2006)
15. C. Chen, D.H. Zanette, J.R. Guest, D.A. Czaplewski, D. López, Phys. Rev. Lett. **117**, 017203 (2016)
16. D.H. Zanette, Pap. Phys. **9**, 090003 (2017)